CONF-780213--2

PRECIPITATION RESPONSE OF AUSTENITIC STAINLESS STEEL TO SIMULATED FUSION IRRADIATION*

P. J. Maziasz
Metals and Ceramics Division, Oak Ridge National Laboratory
Oak Ridge, Tennessee 37830

ABSTRACT

The precipitation response of annealed type 316 stainless steel irradiated in HFIR is studied and compared to previously observed thermal aging and fast reactor irradiation responses. Irradiation in HFIR simultaneously produces high levels of helium and displacement damage and partially simulates a fusion environment. Samples have been irradiated at temperatures from 550–680°C to fluences producing up to 3300 appm He and 47 dpa. If the precipitation response after HFIR irradiation is compared to that after thermal aging on a time-temperature-precipitation diagram, HFIR irradiation results in similar phase combinations, but shifted to lower temperatures and shorter times relative to thermal aging. The shifts range from 70°C to 200°C and are different for different phase combinations. The phase regions resulting from fast reactor irradiation require little or no shift in temperature or time relative to thermal aging. Therefore, HFIR irradiation also results in shifting the phase regions to shorter times and lower temperatures relative to fast reactor irradiation. The addition of simultaneous

---

*Research sponsored by the Department of Energy under contract with the Union Carbide Corporation.

helium production to the irradiation environment is coincident with the absence of the unidentified rod shape precipitate and the presence of M_6C and Laves phases for HFIR relative to fast reactor irradiation at similar temperatures and fluences. Most voids produced by irradiation in a fast reactor are heterogeneously nucleated on the rod shaped precipitates or $M_{23}C_6$ and after HFIR irradiation only a fraction of the cavities are attached to precipitates with Laves being the most preferred and $M_{23}C_6$ the least preferred. Helium has been shown to change the swelling, mechanical properties and cavity response of annealed type 316 stainless steel relative to fast reactor irradiation. Helium is shown to change the precipitate response as well, and is important in understanding and anticipating fusion environment materials response.

Introduction

Precipitation as a result of phase instability is of concern for materials exposed to various environments during engineering applications. Precipitation is important because it can alter the properties of an alloy. Phase instability and the resulting precipitation reactions, however, are different for different environments. In stainless steels, precipitation accompanies high temperature service or irradiation exposure and can produce several different effects. Precipitation on a fine scale can produce strengthening, but removal of elements that promote solid solution strengthening by coarse precipitation can reduce strength. Fast neutron irradiation can alter the precipitation response by changing the kinetics or by altering the free energies of various phases relative to one another due to the mixing of excess vacancies produced by displacement damage.[1] In addition, precipitation during irradiation, may remove alloying elements that retard swelling when in solid solution and, in some instances, provide additional nucleation sites for voids. In a fusion reactor environment, helium will be produced in addition to displacement damage. Simultaneous production of high levels of helium and displacement damage can simulate a fusion environment and has been shown to change the swelling,[2] mechanical properties,[3] and the cavity component of the microstructural[4] response. It might well be expected to change the precipitation response also. The available literature data on precipitation provides a good base upon which to compare the simulated fusion precipitate response.

The thermal aging response of 316 stianless after solution annealing (1050–1260°C for 1–1.5 hrs) has been consistently characterized by Weiss and Stickler[5] and Spruiell et al[6] for thermal aging temperatures ranging from

480–900°C and for times up to 3000 hr. The compositions of the steels used in both studies are given in Table I. A time-temperature-precipitation (TTP) diagram is a sequence of phase regions defined by the phase combinations observed after isothermal aging for various exposure times. Weiss and Stickler's results are presented in a TTP diagram in Fig. 1, for aging after annealing at 1260°C for 1.5 hr. They also proposed a scheme of phase reactions to explain the phases observed, and this is shown in Fig. 2. $M_{23}C_6$ was found, as shown in Fig. 1, up to 900°C after 1500 hrs. Samples treated above this temperature were not examined, and the upper limit for $M_{23}C_6$ formation was not verified experimentally. $M_{23}C_6$ particles were found to precipitate successively at grain boundaries, twin boundaries, and finally intragranularly. Trace amounts of M_6C were observed after 1500 hr at 650°C. The scheme of Fig. 2 indicates that M_6C forms from $M_{23}C_6$. Sigma phase was observed after 1500 hr at about 820°C and after longer times at lower temperatures. It was observed successively at triple points, grain boundaries, incoherent twin boundaries, and finally on intragranular inclusions. Chi phase, observed after 150 hr at 815°C, had a similar nucleation site sequence to sigma phase. Laves phase, observed after about 150 hr at 730°C was found to precipitate intragranularly and only occasionally at grain boundaries. As observed from Fig. 1, chi and Laves both exhibit C-type curves, and chi is the higher temperature phase of the two. The findings of Spruiell et al. were similar to these. They compared 316 annealed at 1050°C with 316 annealed at 1200°C, and at a carbon content of ∿0.6 w% show that both treatments produce similar microstructures and hence justify comparison with Weiss and Stickler who annealed their material at 1260°C.

The fast reactor response of solution annealed (1/2–1 hr at 1050°C) type 316 has been examined by Bloom and Stiegler,[7] Leitnaker et al,[8] and Brager and Straalsund[9] after irradiation in the Experimental Breeder Reactor-II

(EBR-II) and by Barton et al[10] after irradiation in the Dounreay Fast Reactor (DFR). The compositions of these steels are given in Table I. Collectively, those authors examined 316 stainless steel irradiated at 380–850°C at fluences producing up to ∿30 dpa (for times up to ∿7500 hrs) and ∿5 appm He. All agreed that there was no precipitation of $M_{23}C_6$, M_6C or the intermetallic phases below 425°C. Cawthorne and Brown,[11] however, observed a fine gamma-prime phase after irradiation at 270–540°C in DFR. The precipitate density was 0.8–4.2 × 10^{15} ppts/cm^3 and the particles ranged from 80–230 Å in diameter. Brager and Garner[12] also observed gamma-prime in 316 after irradiation at 475°C in EBR-II and identified it by energy dispersive x-ray analysis as Ni_3Si. Ni_3Si was found after thermal aging of 316. $M_{23}C_6$ was found generally at the grain boundaries after irradiation at 425–750°C and also intragranularly above 500–525°C. The precipitate density of intragranular $M_{23}C_6$ after irradiation at 580–700°C to ∿10 dpa was 1-2 × 10^{12} ppts/cm^3, as observed by Bloom and Stiegler. An unidentified rod or needle-like precipitate was observed by all investigators for irradiation temperatures from 425–750°C, except for Bloom and Stiegler, who do not see it until ∿580°C. The needle axis was parallel to [100] γ in the matrix, and Bloom and Stiegler observed a precipitate density of 4 × 10^{13} ppts/cm^3 after irradiation at ∿580°C to ∿10 dpa. This phase which does not appear during thermal aging of 316, was observed by Brager and Straalsund to dissolve after post irradiation annealing at 800°C. After irradiation at 750°C, Brager and Straalsund identified massive, isolated rods of chi phase, and Bloom and Stiegler reported metallographic observation of sigma phase at the grain boundaries. Laves phase and M_6C were not reported by any of these investigators. Voids were generally associated with the rod shaped precipitates and at higher temperatures with $M_{23}C_6$ also. Only Bloom and Stiegler noted extensive void association with $M_{23}C_6$.

Table I. Compositions of Stainless Steel in (w %)

Alloy	Reference	Cr	Ni	Mo	Mn	Ti	Si	C	P	S	N	B	Cu	Fe
316	Weiss et al.[5]	17.4	12.3	2.05	1.57	—	0.21	0.066	—	—	—	—	—	balance
316	Spruiell et al.[6]	17.3	13.3	2.33	1.72	0.003	0.40	0.06	0.012	0.007	—	—	—	"
316	Bloom et al.[3,7] & this work	18.0	13.0	2.58	1.90	0.05	0.80	0.05	0.013	0.016	0.05	>0.0005	—	"
316	Brager et al.[9]	17.8	13.55	2.33	—	—	0.30	0.052	0.12	0.020	0.047	>0.0005	0.2	"
316	Barton et al.[10]	17.3	11.4	2.5	1.54	—	0.32	0.039	0.011	0.003	0.023	0.0018	—	"

If the data after fast reactor irradiation are compared to those of thermal aging for similar exposure times, $M_{23}C_6$, sigma, and chi phases appear after fast reactor irradiation at about the same or slightly lower temperatures and on the same nucleating sites as after thermal aging. Laves phase and M_6C are present after thermal aging, but have not been reported after fast reactor irradiation. Ni_3Si and the unidentified rod shaped phase are present after fast reactor irradiation, but are not found after thermal aging. A temperature shift of no more than 50°C gives coincidence of the phase regions for fast reactor irradiation compared to thermal aging.

Simultaneous helium and displacement damage production during irradiation simulating a fusion environment as mentioned above, have been shown to change the swelling,[2] mechanical properties,[3] and microstructural[4] responses of 316 stainless steel relative to fast reactor irradiation which produces displacement damage with very little helium. Helium may well be expected to change the precipitation response also. Calculations[13,14] have shown that helium is very effectively trapped in vacancies and He-vacancy complexes. This is supported experimentally by helium release measurements.[14] A single helium atom in a vacancy may not prevent free recombination of Frenkel pairs, but several helium atoms may introduce a barrier to the process.[13] Thus the fraction interstitials recombining with vacancies would decrease, while the fraction precipitating in matrix as second phases or interstitial loops would increase. The fraction migrating to existing sinks would increase as well. Also, the fraction of vacancy clusters reaching precipitated interstital clusters would be reduced due to decreased mobility of the vacancy clusters with helium in them as will their progressive immobilization by agglomeration into gas filled clusters of larger size. These processes may shift or alter the free energies of the various phases differently during fusion irradiation relative to thermal aging, or to fast reactor irradiation.

These processes may shift or alter the free energies of the various phases differently during fusion irradiation relative to thermal aging, or to fast reactor irradiation. It is, therefore, desirable to study the precipitation response after irradiation in the High Flux Isotope Reactor (HFIR), which produces high levels of helium and displacement damage simultaneously, and compare it to thermal aging and fast reactor results.

Experimental

The composition of the type 316 stainless steel used in this investigation is given in Table I. The final sample preparation involved a 50% reduction in area by swaging, machining into tensile specimens, and annealing for 1 hr at 1050°C, before irradiation in HFIR. The details of the irradiation experiments in HFIR have been reported[2,3,4] and will be summarized here. The irradiation temperatures were calculated based upon a known heat transfer geometry and calculated values of nuclear heating calibrated against measurements using SiC temperature monitors. Uncertainties in the actual irradiation temperature arise from assumptions about the nuclear heat generation in the irradiated material used to calculate the irradiation temperature. The uncertainty in temperatures may be 50–75°C depending upon the nuclear heating values used, the swelling of the specimens, and the average power level of the HFIR per cycle. Helium concentrations were interpolated from calibration curves fitted to data measured by vacuum fusion and mass spectrometry on selected samples. The dpa levels were calculated from the model recommended by the Specialists Meeting on Radiation Damage Units of the International Atomic Energy Agency.[15] The irradiation parameters are given in Table II.

Microscopy disks were cut from the gage sections of tensile specimens. In some cases the specimens had been tensile tested near the irradiation temperatures.

Table II. HFIR Irradiation Parameters

Sample Condition	Irrad. Temp. °C	Neutron Flux E > 0.1 MeV ($\times 10^{15}$ n/cm^2 sec)	Neutron Fluence (E > 0.1 MeV) ($\times 10^{22}$ n/cm^2)	Displacement Damage (dpa)	Helium Content (appm)
Annealed 316	550	0.95	6.18	42	3000
" "	600	1.40	4.21	30	2000
" "	680	1.38	6.91	47	3300

The stainless steel disks were thinned using the two step thinning process described by DuBose and Stiegler.[16] They were examined using JEOL 100-C (120 kV) and Hitachi 1000 (1 MeV) transmission electron microscopes (TEMs) both equipped with side entry double-tilt holders. Good tilting capability was essential to identify the precipitates and establish their habits relationships. Precipitates were identified by tilting to at least three low order zones making use of the kikuchi line pattern and by matching the interzone angles to the tilted angles and the diffracting planes and their included angles within each zone to reported crystallographic data.[17] The orientation relationships were also obtained from the diffraction patterns and illustrated by plotting the stereographic projection of the precipitate phase of the F.c.c. matrix (001) stereographic projection. Chemical analysis was attempted using the JEM 100C TEM equipped with an energy dispersive X-ray spectrometer and STEM attachment. However, the residual gamma radiation due to neutron activation of the steel in HFIR resulted in such a large background count rate that reliable analysis was precluded. Chemical analysis will be performed on extraction replicas which result in low residual activity.[18]

Three annealed 316 samples irradiated in HFIR from 550–680°C to 2000–3300 appm He and 30–47 dpa, as well as two unirradiated samples of annealed 316 aged for 10,000 hr at 600°C and 650°C were examined in this study.

Results

The experimental conditions and phases observed are presented in time, temperature, precipitation (TTP) diagrams in Figs. 1 and 3, and are summarized in Table III. The orientation relations of the precipitate phases relative to the austenite (face-centered cubic) matrix are presented in Figs. 4 and 5 and summarized in Table IV.

Table III. Summary of Precipitate Analysis on Aged or Irradiated Type 316 Stainless Steel

Exposure Temperature, °C	Exposure Time, hr	Intergranular Phase[a]	Intragranular Phase	Cavity Association with Intragranular Phase	Cavity Volume Fraction, %
Aged Samples					
600	10,000	$M_{23}C_6$ Type I	$M_{23}C_6$ Type I	-	-
650	10,000	$M_{23}C_6$ Type I Sigma Type II	$M_{23}C_6$ Type I M_6C Type II Laves Types I, II	- - -	- - -
Irradiated Samples					
550	~16,000	$M_{23}C_6$ Type I	$M_{23}C_6$ Type I M_6C Type I, II Laves Type I, II	Little or None Some One large cavity per precipitate	8.5 ± 2.5%
600	~ 7,800	Sigma Type I	Laves Types I, II	High	1.5 ± 0.3%
680	~13,000	Sigma[b]	Chi Type I	Some	7.0 ± 2.5%

[a]Orientation relationships are defined in Table IV and illustrated in Fig. 4 and 5.

[b]Orientation relation was undetermined.

Table IV.

Precipitate Phase	Orientation Relation Type	Parallel Planes	Ratio of Interplanar Spacings ($d'_{ppt.}/d_\gamma$)[a]
$M_{23}C_6$	I	$[100]\ M_{23}C_6 \parallel [100]_\gamma$	$d'_{100}/d_{100} = 2.95$
		$[110]\ M_{23}C_6 \parallel [110]_\gamma$	$d'_{110}/d_{110} = 2.95$
M_6C	I	$(111)\ M_6C \parallel (\bar{1}\bar{1}\bar{1})_\gamma$	$d'_{111}/d_{\bar{1}\bar{1}\bar{1}} = 3.08$
		$(110)\ M_6C \parallel (1\bar{1}0)_\gamma$	$d'_{\bar{1}10}/d_{1\bar{1}0} = 3.08$
	II	$(101)\ M_6C \parallel (111)_\gamma$*	$d'_{101}/d_{111} = 3.08$
Laves[b]	I	(00.1)Laves $\parallel (231)_\gamma$*	$d'_{00.1}/d_{231} = 8.04$
	II	(00.1)Laves $\parallel (\bar{3}\bar{1}2)_\gamma$*	$d'_{00.1}/d_{\bar{3}\bar{1}2} = 8.04$
		(21.0)Laves $\parallel (1\bar{1}1)_\gamma$	$d'_{21.0}/d_{1\bar{1}1} = 1.14$
	III	(00.1)Laves $\parallel (1\bar{1}3)_\gamma$	$d'_{00.1}/d_{1\bar{1}3} = 7.13$
		(11.0)Laves $\parallel (110)_\gamma$	$d'_{11.0}/d_{110} = 0.93$
Chi[c]	I	$(011)_\chi \parallel (111)_\gamma$**	$d'_{011}/d_{111} = 3.02$
		$(\bar{1}11)_\chi \parallel (011)_\gamma$**	$d'_{\bar{1}11}/d_{011} = 2.01$
		$(0\bar{1}1)_\chi \parallel (0\bar{1}1)_\gamma$**	$d'_{0\bar{2}2}/d_{0\bar{1}1} = 5.0$
Sigma[d]	I	$(001)_\sigma \parallel (1\bar{1}1)_\gamma$	$d'_{001}/d_{1\bar{1}1} = 2.21$
		$(110)_\sigma \parallel (110)_\gamma$	$d'_{220}/d_{110} = 4.91$
		$(1\bar{1}1)_\sigma \parallel (1\bar{1}0)_\gamma$	$d'_{2\bar{2}2}/d_{1\bar{1}0} = 2.90$
	II	$(110)_\sigma \parallel (1\bar{1}1)_\gamma$	$d'_{110}/d_{1\bar{1}1} = 3.0$
		$(100)_\sigma \parallel (\bar{1}10)_\gamma$	$d'_{100}/d_{\bar{1}10} = 3.46$

[a] γ is f.c.c. with $a_0 = 3.6$ Å

[b] Laves d values of interplanar spacing are taken from Andrews et al.

[c] Fe, Cr, Mo chi phase, with d calculated from $a_0 = 8.88$ Å from Weiss and Stickler.[5]

[d] Fe, Cr, Mo sigma phase, with d calculated from $a_0 = 8.88$ Å, $C_0 = 4.6$ Å from Weiss and Stickler.[5]

* - not exactly parallel, a slight angular displacement.

** - several degrees from not being parallel.

The phase boundaries on the TTP curve determined by data taken by Weiss and Stickler[5] have been extended to longer aging times in order to represent data taken in this work at 600 and 650°C after aging for 10,000 hr. In some cases the curves were slightly altered, within the scope of Weiss and Stickler's data points, in order to be consistent with the phase reaction scheme proposed by them (see Fig. 2). In particular, the phase region of M_6C was added, because Weiss and Stickler indicate observing trace amounts of M_6C after aging at 650°C for 1500 hr and longer but did not include it in their TTP diagram. The data of Weiss and Stickler were taken for 316 that had been annealed at 1260°C to produce a large grain size (average grain diameter of ∿560 μm). Data in this work were taken for 316 annealed at 1050°C for 1 hr as the final step in the fabrication procedure established to produce an order of magnitude smaller grain size (average grain diameter of ∿55 μm). The fabrication steps of the 316 in this work however included solution annealing for one hour at 1200°C followed by 40–50% reduction in area by swaging at room temperature, prior to the final cold work and solution anneal mentioned above. It is, therefore, reasonable to assume that the amount of carbon in solution, and the homogeneity of its distribution within the grains was about the same as in Weiss and Stickler's specimens so that comparison of this data with their data is legitimate. Furthermore, Spruiell et al.[6] found little difference in precipitation behavior for solution anneals of 1050°C and 1200°C.

In this work, aging at 600°C for 10,000 hrs produced $M_{23}C_6$, (see Fig. 6) and aging at 650°C for 10,000 hrs produced $M_{23}C_6$, Laves, occasional sigma particles and small amount of M_6C (see Fig. 7). These observations are consistent with Weiss and Stickler's reaction scheme for these temperatures and therefore warrant extension of their TTP diagram to include these data. These samples were the control samples for the annealed 316 samples irradiated in HFIR. Their

compatability with the TTP diagram justifies comparison of the HFIR irradiated samples with this diagram.

The precipitation response of annealed 316 irradiated in HFIR has been examined for irradiation at 550°C–680°C to fluences producing 30–47 dpa and 2000–3300 appm He. After irradiation in HFIR at 550°C to 42 dpa and 3000 appm He (∿16,000 hrs), $M_{23}C_6$ was found at the grain boundaries and intragranularly; Laves and M_6C were also found intragranularly (see Fig. 8). After irradiation at 600°C to 30 dpa and 2000 appm He (∿7,800 hrs), large isolated sigma phase particles were observed intergranularly, and Laves phase particles were distributed intragranularly (see Fig. 9). After irradiation at 680°C to 47 dpa and 3300 appm He (∿13,000 hrs), large isolated sigma phase precipitates were found intergranularly, and chi phase was found within the grans(see Fig. 10).

A comparison of the phase combinations observed in the 316 samples after HFIR irradiation with the phase regions of the TTP diagram is shown in Fig. 3. The most significant point is that there are phase regions in the TTP diagram that predict the same phase combinations observed after HFIR irradiation. Coincidence of the points and the appropriate regions on the TTP diagram require a shift of the points both upward in temperature and outward in time relative to thermal aging results. However, the shift is different for each sample, suggesting that irradiation has shifted the free energy curves relative to their unirradiated values by different amounts for each phase. For the sample irradiated at 550°C, a shift of ∿70°C upward in temperature is needed to obtain the appropriate phase region on the TTP diagram. The sample irradiated at 600°C requires consideration of both the TTP diagram and of Weiss and Stickler's reaction scheme shown in Fig. 2. The curve on the TTP diagram corresponding to the beginning to transform to sigma, and at higher temperatures, to sigma plus chi. If $M_{23}C_6$ is a metastable phase, then from Weiss and Stickler's reaction scheme it is logical to assume that

at some later time the transformation will be complete. This means that at some later time, a sigma + $M_{23}C_6$ + Laves phase region in the TTP curve will cross a boundary signifying the end of the tranformation o $M_{23}C_6$ to sigma, giving a sigma + Laves phase region. Thus, the sample irradiated at 600°C would require a shift of ∿90°C upward in temperature and a shift outward in time to get to an appropriate phase region on the TTP diagram. The sample irradiated at 680°C requires an upward shift of ∿200°C on the TTP diagram in order to coincide with the appropriate phase region.

The temperature shifts are approximate and are of course based upon the assumption that the calculated irradiation temperatures are correct. Until experiments with more accurate temperature control are available, some shifts in the irradiation temperature due to experimental uncertainty must also be considered as a possibility to explain the data. It is clear that a uniform shift in either time or temperature is insufficient to bring coincidence of all the irradiated samples with similar phase regions on the TTP diagram. Rather, different shifts are required for each sample, and each sample has different phases present. It therefore seems as though the kinetics and thermodynamics of each phase or phase combination are affected differently by the irradiation. The net result of simulated fusion irradiation at these temperatures and fluences seems to be shifting the phase regions similar to those observed after thermal aging on the TTP diagram, to some lower temperature and shorter time. This is in contrast to fast reactor irradiation, where phases not observed under any aging conditions are found after irradiation, but little or no temperature shifting for otherwise similar phase regions is required.

The orientation relations (OR's) for the phases observed after thermal aging and after HFIR irradiation were easily obtained from the electron diffraction patterns necessary to identify a particular phase type. The orientation relations are obtained by noting coincidence or angular displacement, as measured

by tilt angle and Kikuchi band patterns, of the precipitate zones and the matrix zones. Further information is obtained by measuring angles between precipitate and matrix reflections in each low order zone. These orientation relationships are plotted in terms of coincident stereographic projections of each precipitate phase relative to the standard (001) matrix projection in Figs. 4 and 5. They can usually be summarized in terms of several low order matrix and precipitate planes being parallel. The ratio of precipitate to matrix d-spacings for parallel low order planes are very nearly integer values. These ratios are shown in Table IV. This behavior is also noted by Bentley and Leitnaker[19] for sigma phase in type 321 stainless steel. It may well explain why a particular orientation relationships is observed for a particular precipitate phase. The orientation relations for $M_{23}C_6$, chi and sigma OR-I are consistent with data reported by others. The other relationships observed have not been reported. M_6C OR-I and Laves OR-I were found only after HFIR irradiation. Laves OR-III was found only after thermal aging. All other orientation relationships were unaffected by irradiation in the HFIR.

If we compare similar phase regions on the TTP diagram for aged samples and those irradiated in HFIR, HFIR irradiation has changed the morphology and number density of a particular phase as compared to thermal aging. Compare the sample aged 10,000 hrs at 650°C (Fig. 7) and the sample irradiated for ∿16,000 hrs at 550°C (Fig. 8). Figures 7a and 8a show similar $M_{23}C_6$ precipitation at the grain boundary for the aged and irradiated samples respectively. Within the grains, however, $M_{23}C_6$ has changed from narrow laths to square plates or chunks after irradiation (Fig. 7b and 8b and d). Laves appears similar to thermal aging, except that the laths are narrower after irradiation (Fig. 7c and 8c). The precipitate densities of $M_{23}C_6$ and Laves have increased by nearly an order of magnitude due to irradiation, as compared to thermal aging. The amount of M_6C

relative to $M_{23}C_6$ and Laves also seems to have increased as a result of irradiation.

The association between cavities and the various precipitate phases is shown in Figs. 8, 9, and 10. The cavities have previously been shown to be consistent with equilibrium helium bubbles.[4] There seems to be some cavity association with nearly every intra- or intergranular phase, but the highest cavity association in annealed 316 is clearly with Laves phase at 600°C (Fig. 9b). The behavior of Laves has changed from association of several large cavities per precipitate at 550°C to the association of many smaller cavities with each precipitate at 600°C (Fig. 8c compared to 9b). Intragranular $M_{23}C_6$ seems to have the lowest cavity association (Fig. 8b).

Discussions

The results, summarized briefly, show that HFIR irradiation of annealed 316 at temperatures from 550–680°C results in the precipitation of phases similar to those produced by thermal aging if compared to samples aged at higher temperatures and, in some cases, longer times. This is not the case after fast reactor irradiation, where phases are produced that do not occur under any thermal aging conditions. Figure 3 shows a cross-hatched region of the TTP diagram corresponding to times and temperatures observed after fast reactor irradiation. For fast reactor irradiation of annealed 316, Ni_3Si and the unidentified rod shaped precipitate are observed, phases that are not observed after thermal aging to any time and temperature. $M_{23}C_6$, sigma and chi phases are observed after fast reactor irradiation and after thermal aging, with not much of a shift in temperature or time relative to the TTP diagram. M_6C and Laves phases are not reported. If they are absent, it is significant because then not only has irradiation caused the presence of new phases, but has also resulted in the absence of phases normally observed after thermal aging.

Comparison of the results of fast reactor irradiation and HFIR irradiation helps to understand the role that helium plays in changing the radiation response

of precipitation. Fusion reactor environments will produce helium and displacement damage simultaneously whereas fast reactor environments produce displacement damage with very little helium production. Service in both environments includes elevated temperatures. Helium has been demonstrated to change the mechanical properties and swelling of annealed 316.[2,3] Helium has been shown to change the microstructural response of 316 to irradiation,[4] and these microstructures are responsible for the macroscopic properties observed. To predict or understand the response of materials to the fusion environment, it is inadequate to extrapolate fast reactor trends to the fusion case. Comparison of the precipitation response after fast reactor irradiation and after HFIR irradiation leads to conclusions that simultaneous helium + dpa production is involved in the fundamental processes that lead to the development of microstructure during irradiation.

Compare irradiation in HFIR to EBR-II at 550°C. Intra- and intergranular $M_{23}C_6$ are observed in both cases. M_6C and Laves phases are observed intragranularly after HFIR irradiation and are not observed after EBR-II irradiation. An unidentified rod-shaped precipitate is observed after EBR-II irradiation, but not after HFIR irradiation. Compare irradiation in HFIR to EBR-II at 600°C. After fast reactor irradiation, $M_{23}C_6$ is observed intra- and intergranularly along with the unidentified rod-shaped phase. After HFIR irradiation sigma is observed intergranularly and Laves phase intragranularly. Finally, compare irradiation in HFIR to that in EBR-II at 680°C. Again, intra- and intergranular $M_{23}C_6$ and the rod-shaped precipitate are observed after irradiation in EBR-II, and sigma and chi phases are found along with these phases at 750°C. After irradiation in HFIR, only sigma is observed at the grain boundaries and chi phase is observed intragranularly. For EBR-II irradiation, the phases $M_{23}C_6$, sigma and chi appear at times and temperatures consistent with equivalent thermal

aging. In HFIR, as mentioned previously, a shift in temperature and/or time is required for coincidence of similar phase regions. Since irradiation temperatures in both reactors are calculated without the benefit of verifying measurements, these comparisons are not absolute but rather assume correctness of the irradiation temperatures. But the differences are great enough to justify the conclusion that the production of helium during the irradiation has changed the precipitation response of annealed 316.

Not only has the precipitation response changed, but the cavity association with precipitates is also different after irradiation in HFIR as compared to EBR-II. Voids are associated with the unidentified rods and $M_{23}C_6$ after irradiation in EBR-II. Both Brager and Straalsund,[9] and Bloom and Stiegler[7] indicate that nearly all voids are attached to precipitates. After HFIR irradiation, cavities are attached to nearly all precipitate phases, but only a fraction of the total number of cavities is attached to precipitates rather than dislocations in the matrix of annealed 316. Since the HFIR case the cavities are most probably equilibrium helium bubbles, the cavity association is an indication of the helium accommodation of the various phases. Laves phase has several large cavities per precipitate at 550°C (see Fig. 7c) and many smaller cavities per precipitate at 600°C (see Fig. 8b) after HFIR irradiation. It seems that of the phases present in annealed 316, Laves accommodates helium most effectively. However, Maziasz and Bloom[20] have shown that even in the presence of Laves phase, nearly exclusive association of very small cavities with TiC occurs when 0.23 wt % Ti is added to annealed 316. Laves is not the best possible, but the best available phase to accommodate helium is annealed 316.

Annealed 316 is not the prime candidate for the first wall of a fusion reactor. However, stainless steel alloys that are composition or preirradiation microstructural variations of 316 are likely candidates. They have been chosen

based on improvements relative to annealed 316, and the improvements are consistent with microstructural changes observed. The effect of irradiation on the various components of the microstructural response will determine what combination of preirradiation microstructure and alloy chemistry will produce the optimum response. Precipitation is a portion of this response and understanding and characterizing it will help the optimization process.

Summary and Conclusions

1. Curves drawn from the data of Weiss and Stickler on a TTP diagram for annealed 316 have been extrapolated to longer aging times. The shape of portions of their curves have been altered slightly as well as extended, and and M_6C phase region has been included to be consistent with their phase reaction scheme and their data. These curves were then extended to longer aging times; no unreasonable changes were necessary to include the present data for aging at 600 and 650°C for 10,000 hr.

2. The precipitates identified in samples of annealed 316 irradiated in HFIR are compared to the TTP diagram for aging at similar times and temperatures. Phase regions not inconsistent with the phase combinations observed after HFIR irradiation can be obtained by considering the extended TTP diagrams and Weiss and Stickler's phase reaction scheme. The appropriate phase regions on the TTP diagram are shifted upward in temperature and/or to longer times relative to HFIR irradiation times and temperatures. The shifts appear to be different for different phases.

3. The orientation relationships for the crystal structure of precipitate phases relative to the matrix have been determined for both aged and HFIR irradiated samples. The orientation relationships are plotted stereographically relative to the (001) projection of the matrix. The orientation relationships

are plotted stereographically relative to the (001) projection of the matrix. The orientation relationships for sigma, chi, and $M_{23}C_6$ have been entirely or partially reported in the literature. M_6C OR-I and Laves OR-I were found only after irradiation in HFIR. Laves OR-III was found only after thermal aging. The other orientation relations were unaffected by irradiation in HFIR.

4. If similar phase regions are compared for thermal aging and HFIR irradiation, HFIR seems to change the morphology, to increase the number density by nearly an order of magnitude, and to change the relative amounts of some phases as compared to thermal aging.

5. HFIR irradiated samples of annealed 316 are compared with samples irradiated for similar times and temperatures in fast reactors. HFIR irradiation results in the occurrence of M_6C and Laves phase and the absence of the unidentifed rod shaped phase relative to fast reactor irradiation. If both irradiations are compared to similar phase regions on the TTP diagram, the HFIR results seem shifted to higher temperatures relative to the fast reactor results.

6. The changes in precipitate response are coincident with the inclusion of simultaneous helium production during the irradiation. The cavity interaction and association with the precipitate phases also changes with the addition of helium. After fast reactor irradiation almost all voids are associated with either the rod-shaped phase or $M_{23}C_6$. After HFIR irradiation only a fraction of total number of cavities are associated with the precipitates, but there is some association with nearly every particle present. Laves phase shows the highest cavity association and $M_{23}C_6$ the least in annealed 316 irradiated at 550–580°C for up to 16,000 hr.

Acknowledgements

I would like to acknowledge E. E. Bloom, F. W. Wiffen, J. O. Stiegler for planning and executing the irradiation experiments and for helpful and necessary discussion during writing of this paper. Thanks to J. O. Stiegler for providing some of the micrographs on one of the samples included. Special thanks to John Houston and Bruce Cox for excellent thinning of the samples examined. Thanks to R. W. Carpenter, J. Bentley, E. A. Kenik and L. K. Mansur for productive discussion of several ideas incorporated into this paper. Special thanks to Gail Smith for perseverance and patience in typing this paper.

References

1. Peter Wilkes, "Phase Stability under Irradiation," *Proceedings of Workshop on Correlation of Neutron and Charged Particle Damage, ORNL, Oak Ridge, Tennessee, June 8–10, 1975, Appendix A.*

2. F. W. Wiffen and E. E. Bloom, "Effect of High Helium Content on Stainless Steel Swelling," *Nucl. Tech. 25,* 113 (January 1975).

3. E. E. Bloom and F. W. Wiffen, "The Effects of Large Concentrations of Helium on the Mechanical Properties of Neutron-Irradiated Stainless Steel," *J. Nucl. Mater. 58,* 171 (1975).

4. P. J. Maziasz, F. W. Wiffen, and E. E. Bloom, "Swelling and Microstructural Changes in Type 316 Stainless Steel Irradiated under Simulated CTR Conditions," *Proceedings of International Conference on Radiation Effects and Tritium Technology for Fusion Reactors,* p.I–259, Conf. 750989 (1976).

5. B. Weiss and R. Stickler, "Phase Instability During High Temperature Exposure of 316 Austenitic Stainless Steel," *Met. Trans. 3,* 851 (April 1972).

6. J. E. Spruiell, J. A. Scott, C. S. Ary, and R. L. Hardin, "Microstructural Stability of Thermal-Mechanically Pretreated Type 316 Austenitic Stainless Steel," *Met. Trans. 4,* 1533 (June 1973).

7. E. E. Bloom and J. O. Stiegler, "Effect of Irradiation on the Microstructure and Creep-Rupture Properties of Type 316 Stainless Steel," *Effects of Irradiation on Substructure and Mechanical Properties of Metals and Alloys,* ASTM STP 529, p. 360–382 (1973).

8. J. M. Leitnaker, E. E. Bloom, and J. O. Stiegler, "The Effect of Minor Constituents on Swelling in Stainless Steel," *J. Nucl. Mater. 49,* 57–66 (1973).

9. H. R. Brager and J. L. Straalsund, "Defect Development in Neutron Irradiated Type 316 Stainless Steel," *J. Nucl. Mater 46,* 134–158 (1973).

10. P. J. Barton, B. L. Eyre, and D. A. Stow, "The Structure of Fast-Reactor Irradiated Solution-Treated AISI Type 316 Stainless Steel," *J. Nucl. Mater 67,* 181–197 (1977).

11. C. Cawthorne and C. Brown, "The Occurrence of an Ordered fcc Phase in Neutron Irradiated M316 Stainless Steel," *J. Nucl. Mater. 66,* 201 (1977).

12. H. R. Brager and F. A. Garner, "Swelling as a Consequence of Gamma Prime (γ') and M(C,Si) Formation in Neutron Irradiated 316 Stainless Steel," to be putlished in *Journal of Nuclear Materials.*

13. W. D. Wilson, "The Theory of Diffusion and Trapping of Hydrogen and Helium in Metals, A Review," *Proceedings of International Conference on Fundamental Aspects of Radiation Damage in Metals,* CONF-751006-P2, Vol. ii, p. 1025 (1975).

14. W. Bauer and W. D. Wilson, "Helium Migration in Metals," *Proceedings of International Conference on Irradiation Induced Voids in Metals, Albany, N.Y.,* CONF-710601, p. 230 (1972).

15. "Recommendations for Displacement Calculations for Reactor/Accelerator Studies in Austenitic Stainless Steel," C. Z. Serpan, Chairman, Working Group on Reactor Radiation Measurements, *Nucl. Eng. Des. 33,* 91 (1975).

16. C. K. H. DuDose and J. O. Stiegler, *Semiautomatic Preparation of Specimens for Transmission Electron Microscopy,* ORNL-4066 (February 1967).

17. K. W. Andrews, D. J. Bryson, and S. R. Klown, *Interpretation of Electron Diffraction Patterns,* Adam Hilger Ltd., 2nd Edition, 1971.

18. K. Farrell, J. Bentley, and D. N. Braski, "Direct Observation of Irradiation-Induced Coated Cavities," *Scripta Metallurgica 11,* 243 (1977).

19. J. Bentley and J. M. Leitnaker, "Precipitate Phases in Type 321 Stainless Steel After Aging 17 Years at ~600°C," to be published in the *Proceedings of Symposium on "Metal Physics of Stainless Steels," Denver, Colorado, Feb. 26-March 2, 1978.*

20. P. J. Maziasz and E. E. Bloom, "Comparison of 316 + Ti with 316 Stainless Steel Irradiated in a Simulated Fusion Environment," *ANS Transactions 27,* 268 (1977).

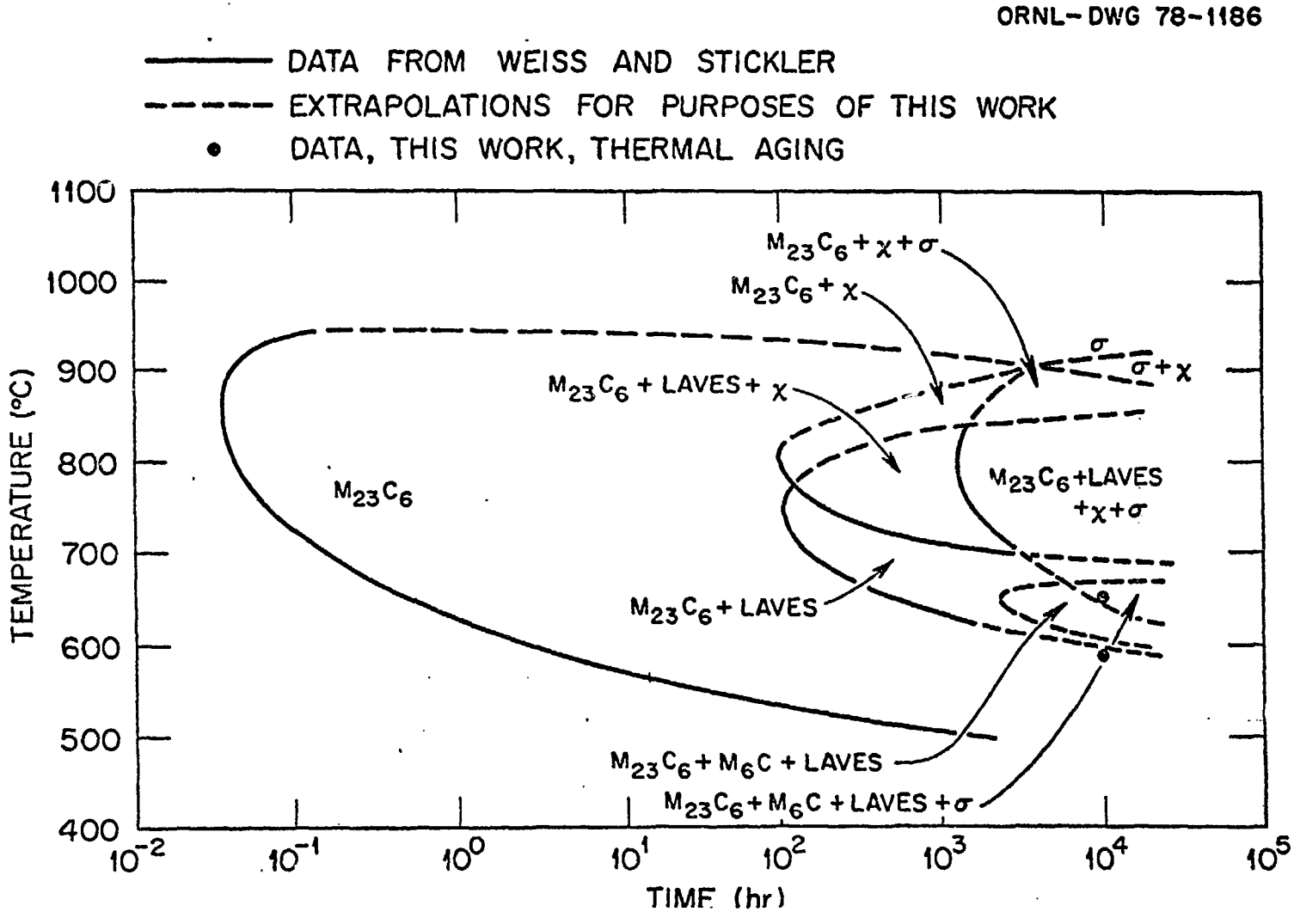

Fig. 1. A TTP diagram for annealed 316 stainless steel. The boundaries of the phase regions taken from data by Weiss and Stickler[5] are extended to longer aging times and to include data from this work.

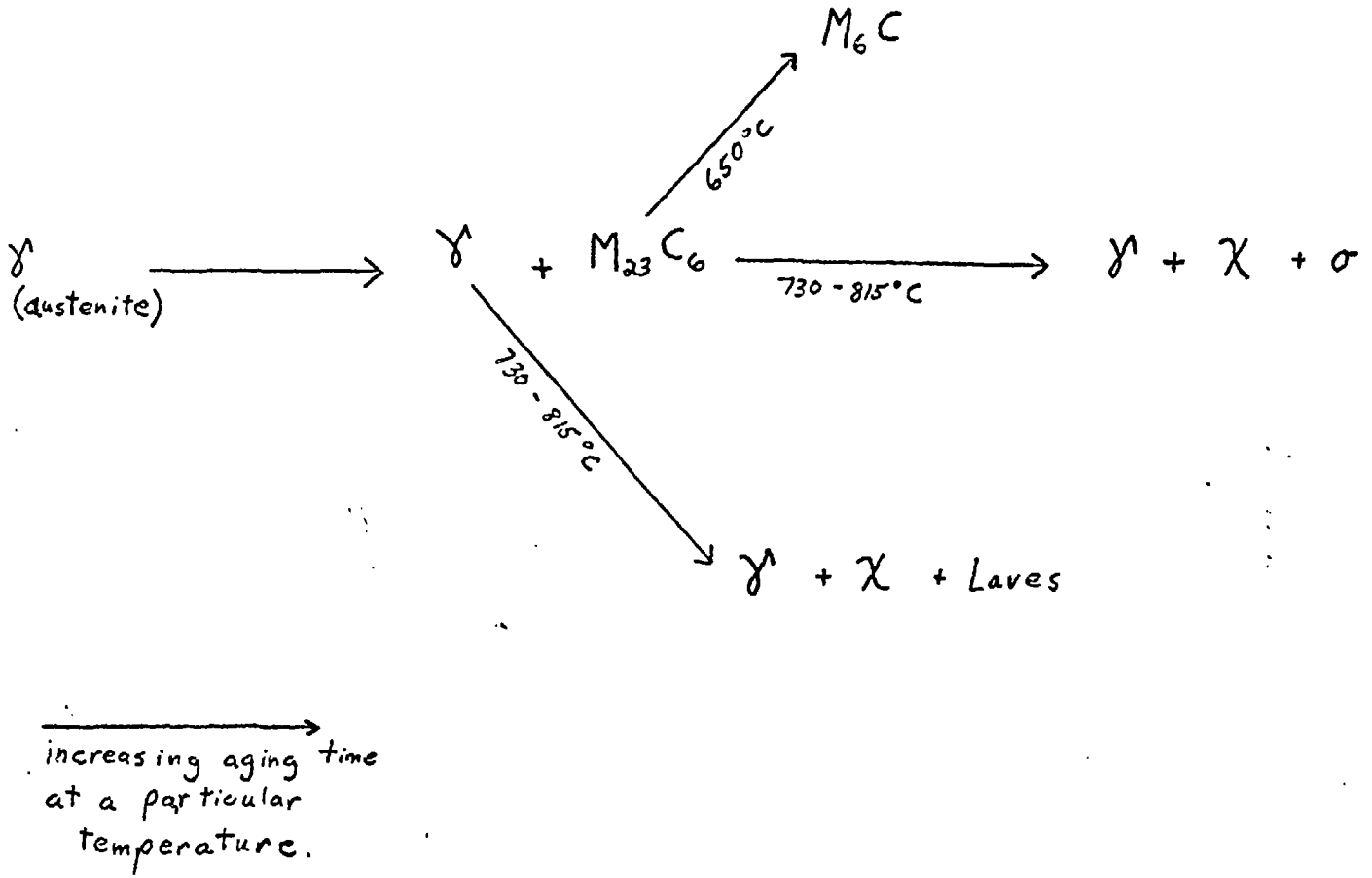

Fig. 2. A schematic diagram of the phase reaction sequence proposed by Weiss and Stickler[5] for annealed 316 stainless steel during aging.

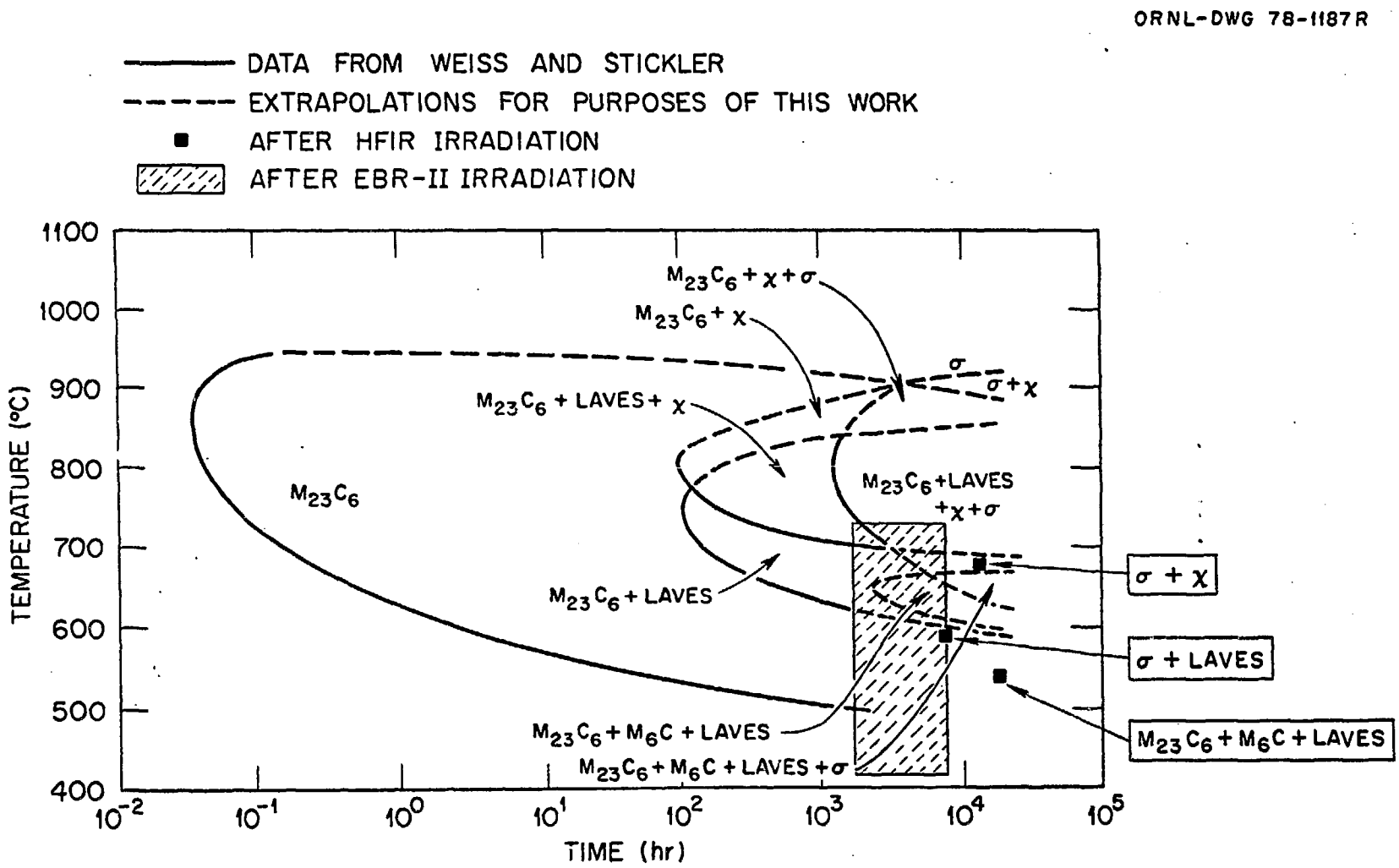

Fig. 3. A TTP diagram of aging results for annealed 316 stainless steel including data obtained after HFIR and EBR-II irradiation. The data are plotted at the irradiation temperatures and times and the phases observed are indicated.

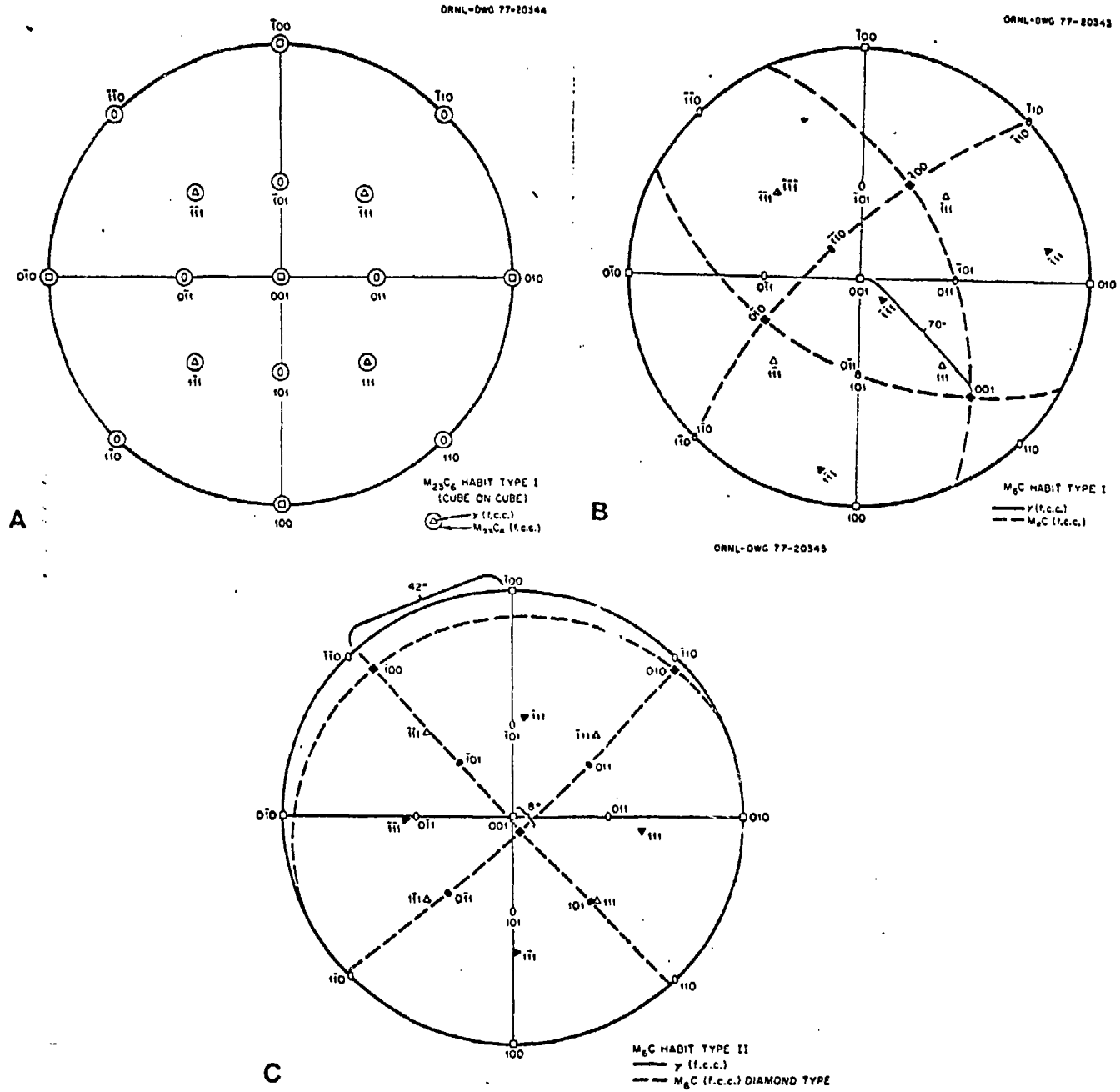

Fig. 4. Stereographic projections of Orientation Relations (OR's) between γ matrix and precipitate planes as determined from electron diffraction. OR's for carbide phases are shown (a–c).

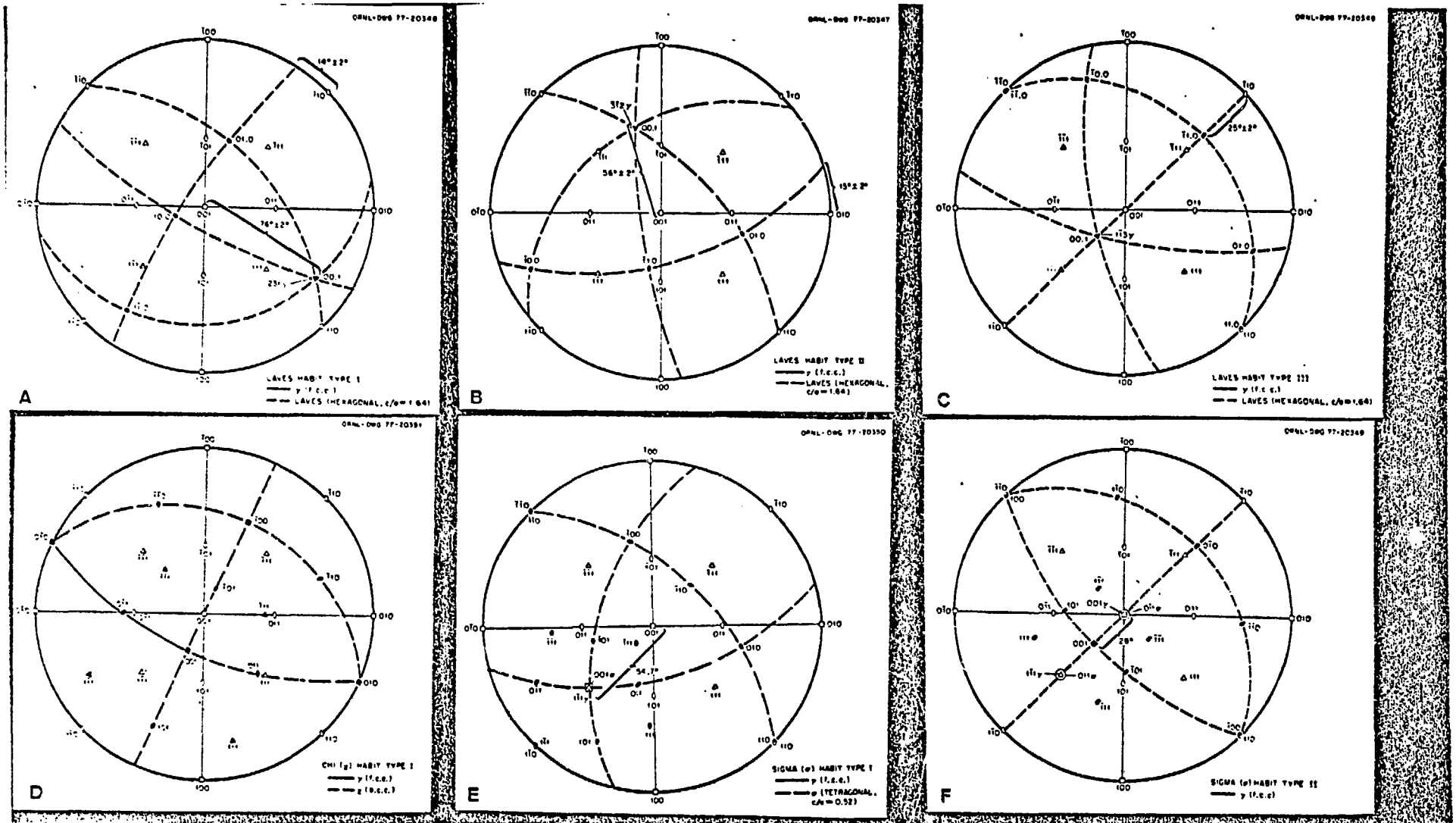

Fig. 5. Stereographic projections of Orientation Relations (OR's) between γ matrix and precipitate planes as determined from electron diffraction. OR's for intermetallic phases are shown (a–g).

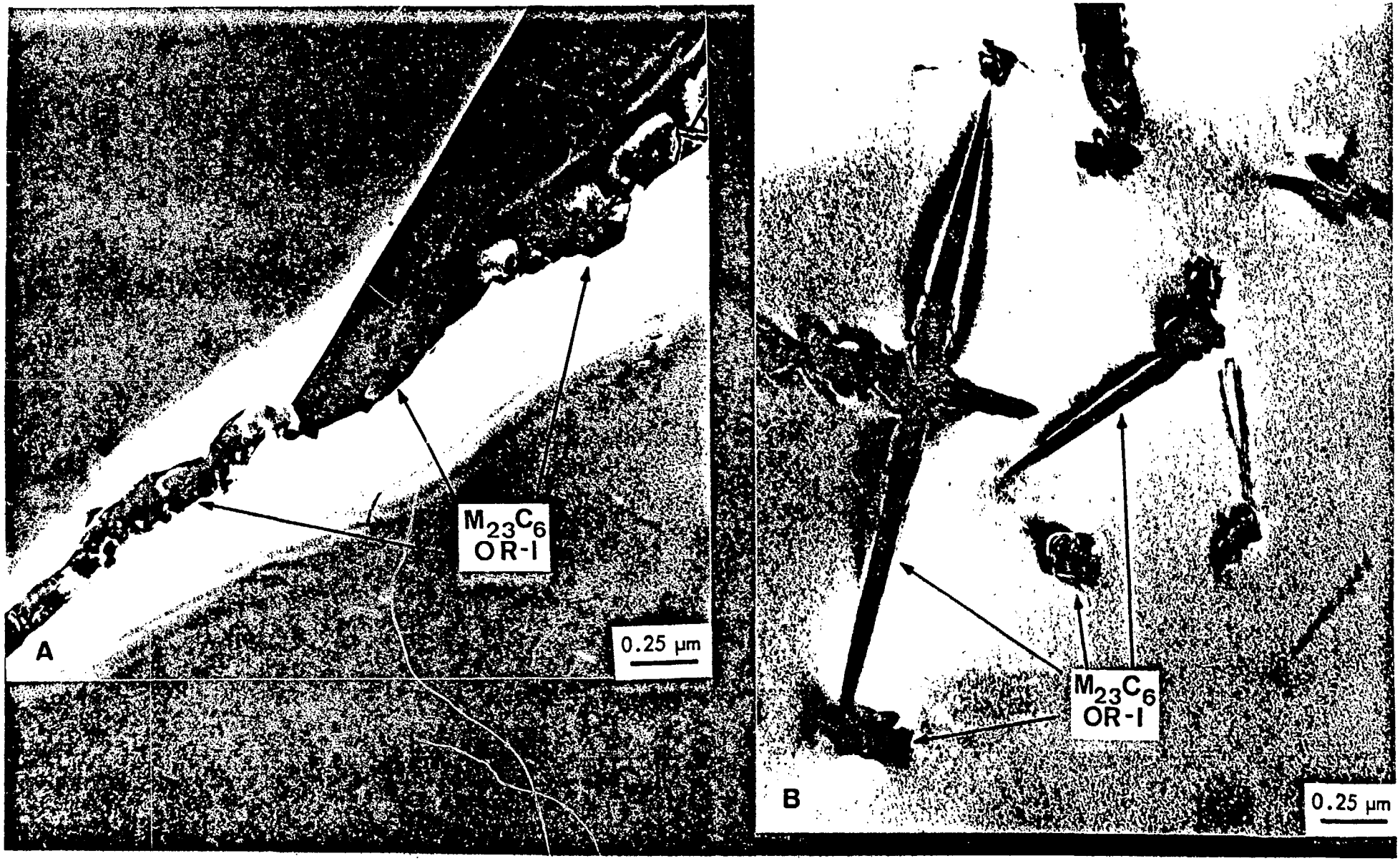

Fig. 6. Annealed (1 hr @ 1050°C) 316, aged for 10,000 hrs at 600°C. a.) high angle grain boundary precipitation of $M_{23}C_6$. Each precipitate is cube on cube with either one grain on the other. b.) Sword-like intragranular $M_{23}C_6$. Precipitate density is $\sim 2 \times 10^{13}$ ppts/cm^3.

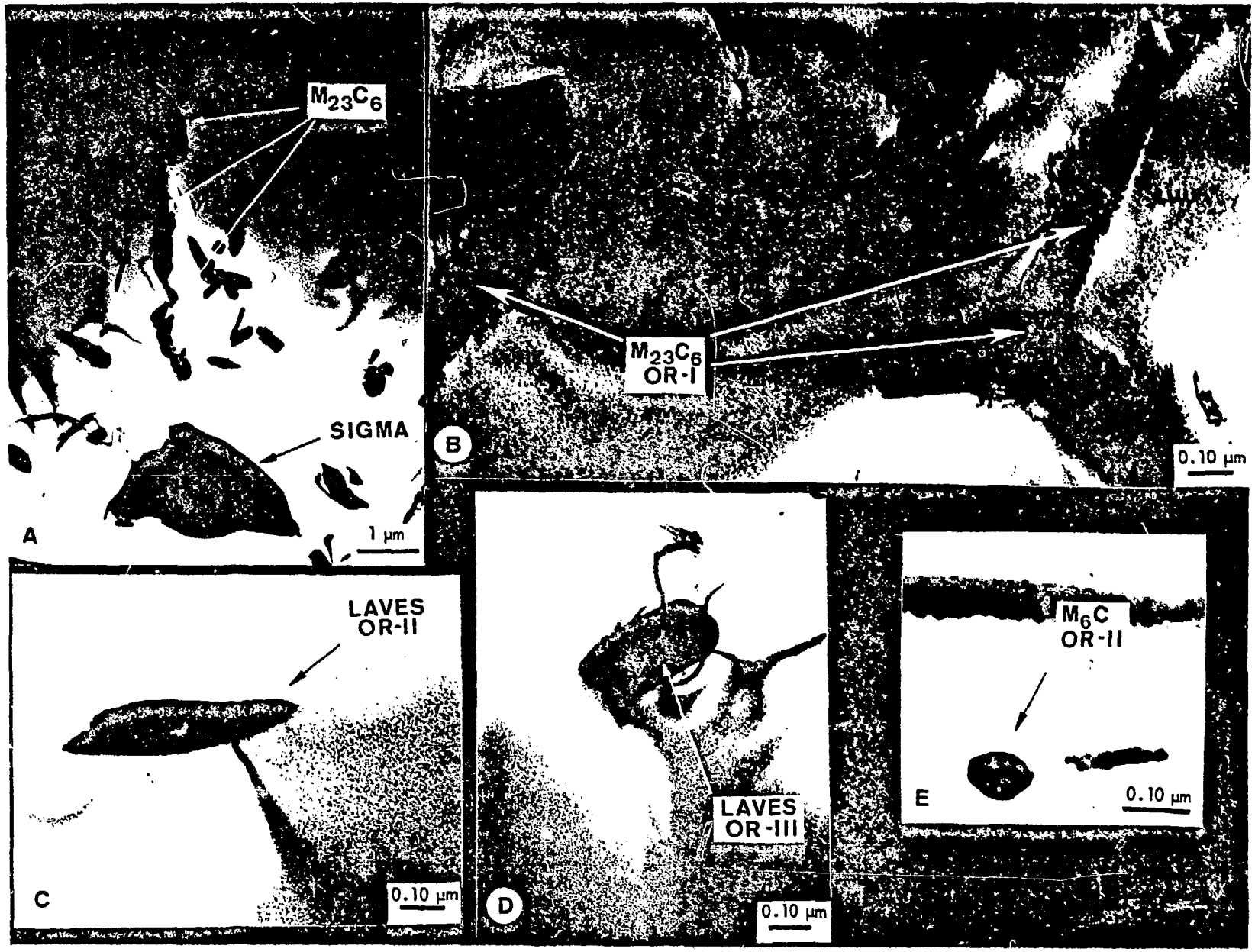

Fig. 7. Annealed (1 hr @ 1050°C) 316, aged for 10,000 hrs at 650°C. a.) Grain boundary with nearly continuous $M_{23}C_6$ and occasional sigma phase particle. b.) $M_{23}C_6$ particles, laths or plates. Beam direction in several degrees from [11$\bar{2}$] with $\underline{g}$ = [$\bar{1}$11], s = 0 in the γ matrix. Precipitate density is ∿5 × 10^{12} ppts/cm^3. c.) Laves phase, thin lath. Precipitate is oriented on a [1$\bar{2}$.1] Laves zone axis. Precipitate density is ∿2 × 10^{12} ppts/cm^3. c.) Laves phase, thin lath. Precipitate is oriented on a [$\bar{1}$2.1] Laves zone axis. Precipitate density is ∿2 × 10^{12} ppts/cm^3. d.) Laves phase, rectangular chunk. Precipitate is oriented on a [1$\bar{2}$.1] Laves zone axis. 3.) Small isolated particle of M_6C, oriented on a [0$\bar{1}$1] precipitate zone axis.

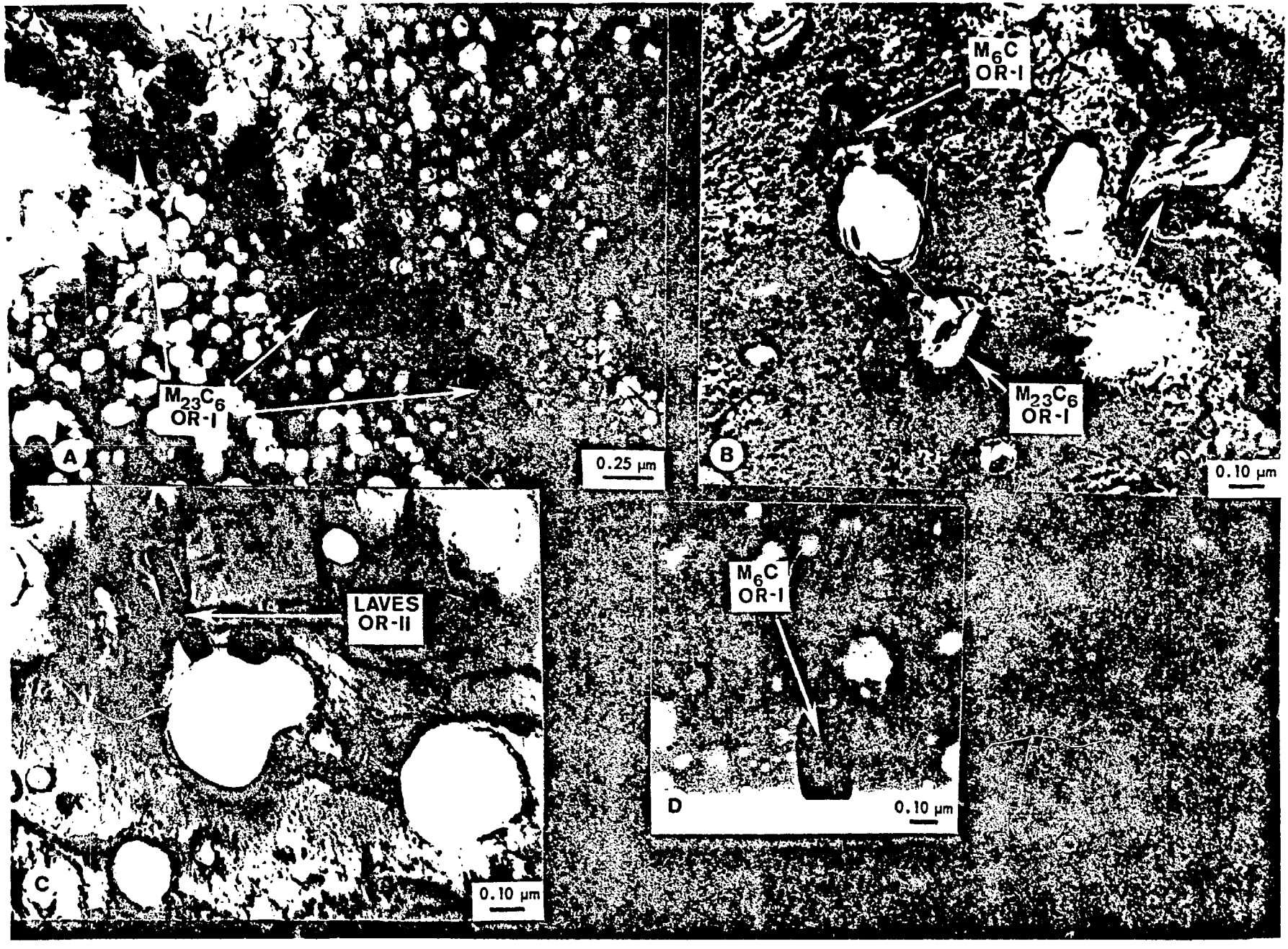

Fig. 8. Annealed (1 hr @ 1050°C) 316, irradiated in HFIR at 550°C to 3000 appm He and 42 dpa (∿16,000 hrs). a.) Grain boundary with nearly continuous $M_{23}C_6$. b.) Intragranular plates of $M_{23}C_6$ and M_6C, both are oriented near [0$\bar{1}$1] precipitate zones, which are coincident with a γ matrix [011] zone axis. Precipitate densities are ∿4 and ∿6 × 10^{13} ppts/cm^3 respectively. c.) Laves phase, thin lath. Precipitate is oriented in a [1$\bar{2}$.0] precipitate zone axis. Precipitate density is ∿2 × 10^{13} ppts/cm^3. d.) Large, isolated M_6C precipitate, oriented on a [1$\bar{3}$4] precipitate zone axis.

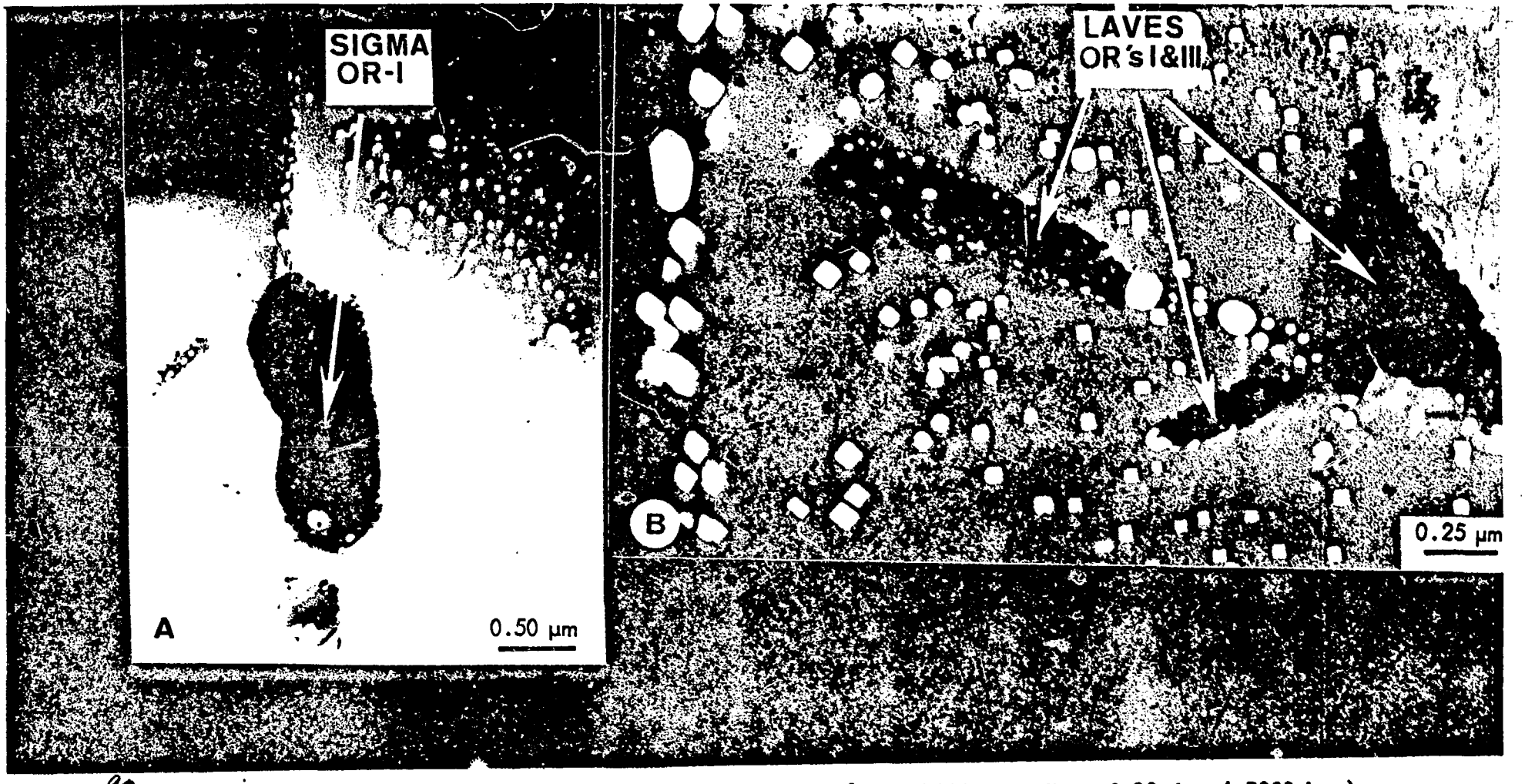

Fig. 6.9 Annealed (1 hr. @ 1050°C) 316, irradiated in HFIR at 600°C to 2000 appm He and 30 dpa (∿7800 hrs). a.) Large, isolated sigma phase particle oriented near a [001] precipitate zone axis which is coincident with a [111] γ matrix zone axis. b.) Cavity coated laths of Laves phase, several of which are oriented near a [00.1] precipitate zone axis. Precipitate density is $\sim 3 \times 10^{12}$ ppts/cm^3.

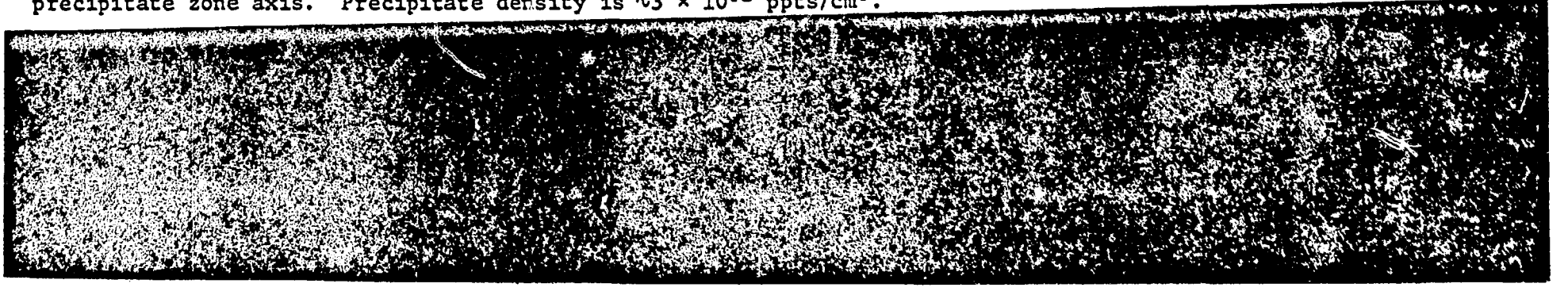

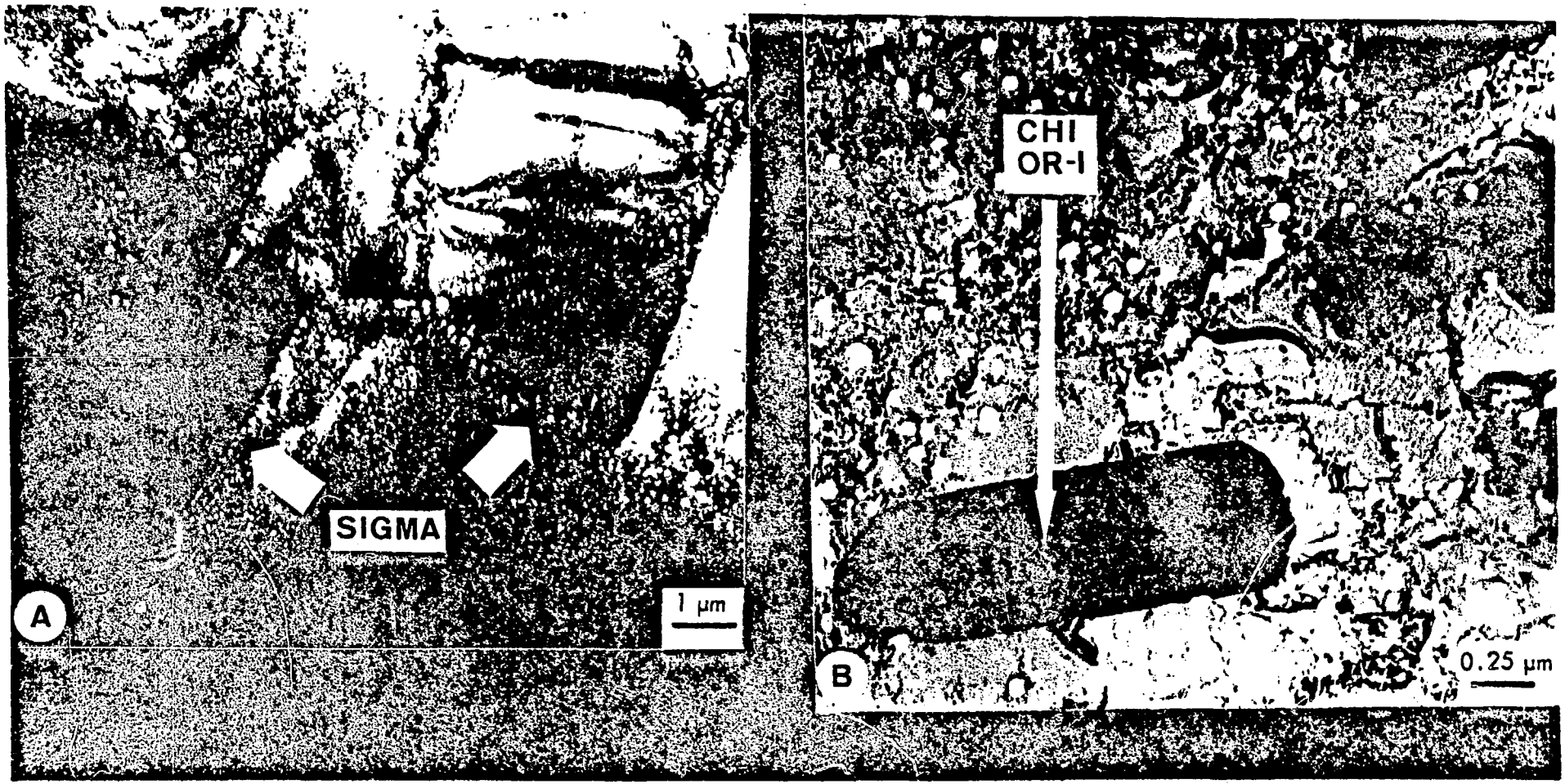

Fig. 10. Annealed (1 hr. @ 1050°C) 316, irradiated in HFIR at 680°C to 3300 appm He and 47 dpa (∿13,000 hrs). a.) Massive sigma phase at the grain boundaries. b.) Large intragranular plates of chi phase. The dark chi phase is oriented on a [6$\bar{8}$1] precipitate zone axis.